NEUROSCIENCE

Specialized cutaneous Schwann cells initiate pain sensation

Hind Abdo[1]*, Laura Calvo-Enrique[1]*, Jose Martinez Lopez[1], Jianren Song[2], Ming-Dong Zhang[1], Dmitry Usoskin[1], Abdeljabbar El Manira[2], Igor Adameyko[3], Jens Hjerling-Leffler[1], Patrik Ernfors[1]†

An essential prerequisite for the survival of an organism is the ability to detect and respond to aversive stimuli. Current belief is that noxious stimuli directly activate nociceptive sensory nerve endings in the skin. We discovered a specialized cutaneous glial cell type with extensive processes forming a mesh-like network in the subepidermal border of the skin that conveys noxious thermal and mechanical sensitivity. We demonstrate a direct excitatory functional connection to sensory neurons and provide evidence of a previously unknown organ that has an essential physiological role in sensing noxious stimuli. Thus, these glial cells, which are intimately associated with unmyelinated nociceptive nerves, are inherently mechanosensitive and transmit nociceptive information to the nerve.

The ability to detect and protect from damage-causing (noxious) stimuli relies on the existence of sensory afferents, called nociceptors (*1*–*6*). Nociceptive nerves are generally unmyelinated and associate with Remak glial cells that protect and metabolically support the axons (*7*, *8*). The unmyelinated nerve endings are activated by noxious stimuli and, hence, represent the pain receptors in the skin. We used genetic labeling to address how cutaneous glia (Schwann cells) distribute and interact with nociceptive nerve terminals. Neural-crest and glia-specific Cre lines (Plp-CreERT2, Sox10-CreERT2, Sox2-CreERT2) coupled to the Rosa26-enhanced YFP ($R26R^{YFP}$) or $R26R^{tdTOMATO}$ ($R26R^{TOM}$) reporter lines were used. Recombination in Schwann cells and staining for nerves with PGP9.5 revealed cutaneous Schwann cells in a static location in the dermis, close to the dermal/epidermal border in both glabrous and hairy skin, and were closely associated with ascending nerve fibers in both Plp-YFP (Fig. 1A and fig. S1, A and C) and Sox10-TOM mice. The latter also revealed epidermal Schwann cell processes attached to nerves, likely because of brighter fluorescence (Fig. 1B and fig. S1, B and D). Consistent with Schwann cells, these were Plp^{YFP+}, $SOX10^{+}$, and $S100\beta^{+}$ cells with extensive radial processes into epidermis (Fig. 1A). Transmission electron microscopy revealed that nerve terminals emerged from the soma of Schwann cells located a few micrometers from the border to epidermis with the glia as the only source of cytoplasmic sheaths. Ascending immediate subepidermis nerves branched with radial Schwann cell processes, ensheathing progressively fewer nerves. In intraepidermal endings, smaller parts of nerve terminals were in contact with glia processes (Fig. 1C and fig. S2A). Nerve and Schwann cell processes were surrounded by a thick layer of fibrillar collagen oriented in the direction of the glio-neural complex and distinct from the rest of collagen. These morphologically distinct glia also carried high expression of Aquaporin1 (Fig. 1E) and were associated with $CGRP^{+}$, $P2RX3^{+}$, and transient receptor potential $V1^{+}$ nociceptive fibers (Fig. 1F and fig. S2B). Immunoelectron microscopy for TOMATO in Sox10-TOM mice confirmed Tomato

[1]Department of Medical Biochemistry and Biophysics, Division of Molecular Neurobiology, Karolinska Institutet, Stockholm 17177, Sweden. [2]Department of Neuroscience, Karolinska Institutet, Stockholm 17177, Sweden. [3]Department of Physiology and Pharmacology, Karolinska Institutet, Stockholm 17177, Sweden.
*These authors contributed equally to this work.
†Corresponding author. Email: patrik.ernfors@ki.se

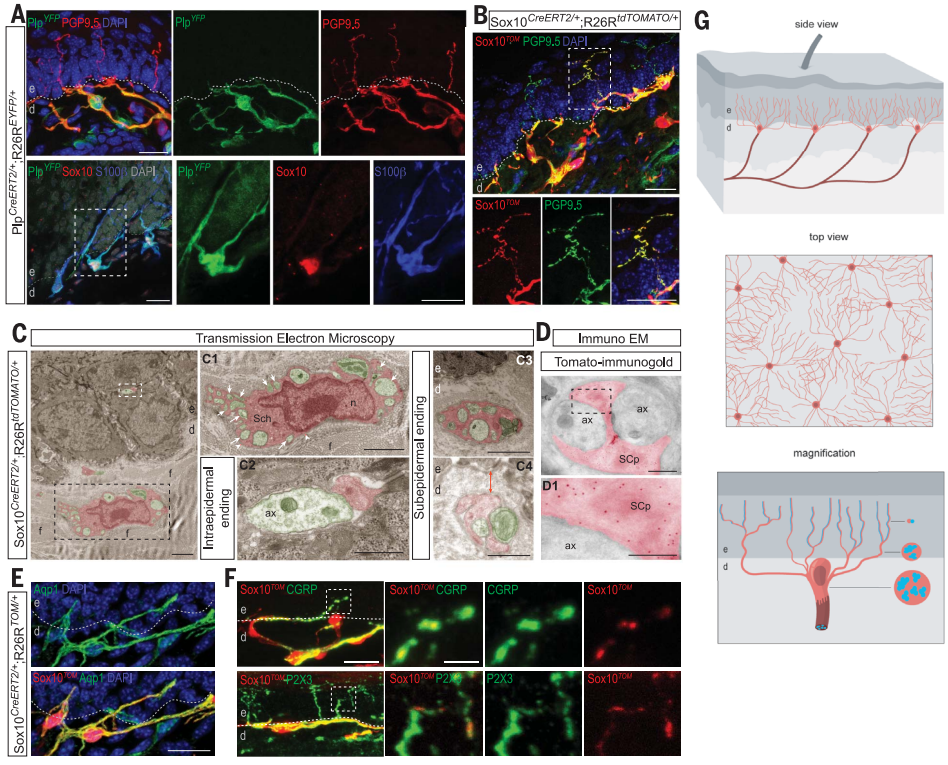

Fig. 1. Cutaneous Schwann cells form a glio-neural end organ in the skin. (**A** and **B**) Cutaneous Schwann cells in the subepidermal border with radial processes into epidermis ensheath unmyelinated nerve endings. Genetically labeled Schwann cells in Plp-YFP (A) and Sox10-TOM (B) mice associate with unmyelinated nerves ($PGP9.5^{+}$) and express glia markers SOX10 and S100β. Insets show higher magnification. (**C** and **D**) Transmission electron microscopy of the glio-neural complex. Images were pseudo-colored (axons, green and cutaneous Schwann cell and its processes, red). (C1) Subepidermal border and (C2) epidermis are higher magnification of boxed area in (C). Arrowheads point to basal lamina on the abaxonal surface, and arrows point to axons. (C3 and C4) Subepidermal Schwann cell processes enfold few (C4) or several axons (C3) close to the epidermis (red arrow is 1 μm in C4). (D) Immuno–electron microscopy (EM) with anti-dsRed antibody (red dots) shows specific expression of TOMATO in Schwann cell process and not by the axons. (**E**) Immunohistochemistry for Aquaporin1 (Aqp1). (**F**) Immunohistochemistry for CGRP and P2X3. (**G**) Schematic illustration of the glio-neural complex in the subepidermal border and epidermis (nociceptive Schwann cell, red and nerves, blue). Hatched line indicates dermal-epidermal border. ax, axon; d, dermis; DAPI, 4′,6-diamidino-phenylindole; e, epidermis; f, fibrillar collagen; n, nucleus; Sch, cutaneous Schwann cell; SCp, Schwann cell process.

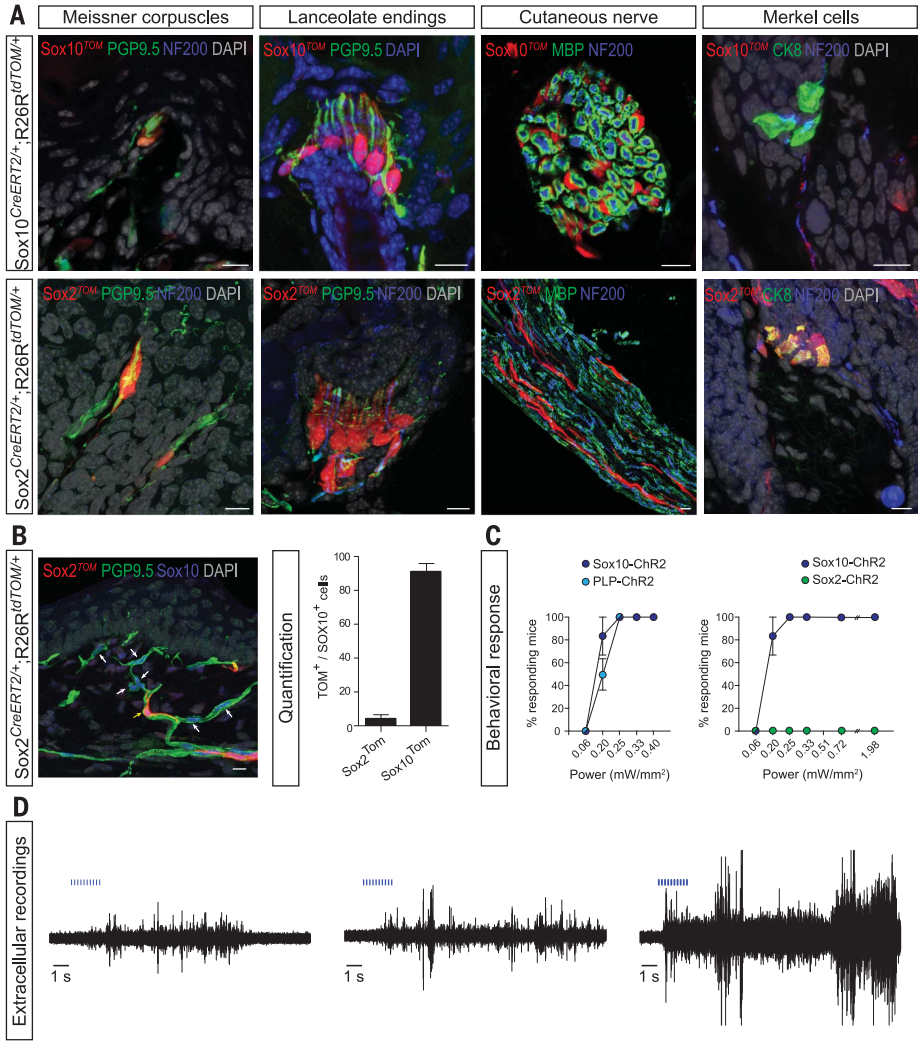

Fig. 2. Nociceptive Schwann cells can initiate pain-like behavior and are sufficient to elicit action potential propagation. (**A**) Immunohistochemistry reveals recombination in LTMR end-organ glia and in Remak glia of nerves in Sox10-TOM and Sox2-TOM mice, and in the latter also in Merkel cells. (**B**) Sox10-TOM but rarely Sox2-TOM mice recombine in nociceptive Schwann cells ($SOX10^+$). White arrows indicate non-recombined and yellow arrow indicates occasional recombined $SOX10^+$ Schwann cell in Sox2-TOM mice. Quantification is on right. (**C**) Optogenetic stimulation of nociceptive Schwann cells results in nocifensive behavior. Sox10-ChR2 and Plp-ChR2 mice but not Sox2-ChR2 mice respond to blue-light application. (**D**) Activation of nociceptive Schwann cells results in nerve electrical activity. Extracellular recording from the palmar nerve after optogenetic stimulation (blue marks) of the skin in Sox10-ChR2 mice. MBP, myelin basic protein; NF200, neurofilament 200.

in ultrastructurally identified glial cells (Fig. 1D and fig. S2C). Thus, a morphologically and molecularly specialized type of Schwann cells (hereafter termed nociceptive Schwann cells) form a mesh-like network in the subepidermal border that constructs a glio-neural complex through an intimate association with nociceptive nerves (Fig. 1G, schematic illustration) that is insulated by structural support of collagen fibers.

To determine whether nociceptive Schwann cells contribute to pain perception, we first analyzed recombination in various glia compartments of Plp-YFP, Sox10-TOM, and Sox2-TOM mice. Both Plp-YFP and Sox10-TOM mice recombine in nociceptive Schwann cells and terminal Schwann cells of Meissner corpuscles, lanceolate endings, and glia in nerves but not Merkel cells or dorsal root ganglion neurons (Fig. 2A and fig. S3). By contrast, Sox2-TOM mice largely failed to recombine nociceptive Schwann cells (Fig. 2B) but recombined in all other compartments seen for Sox10-TOM as well as Merkel cells (Fig. 2A and fig. S4). Thus, if crossed to light-sensitive channels, these driver strains can be used to manipulate Schwann cell activity without direct stimulation of sensory nerves and thereby resolve the role of nociceptive versus other cutaneous Schwann cell types.

The driver strains were crossed to Channelrhodopsin-2 (ChR2)–enhanced YFP mice to generate Plp-ChR2 and Sox10-ChR2 mice. We wanted to determine whether optogenetic stimulation of nociceptive Schwann cells is sufficient to elicit pain-like responses. A light power–dependent increase in limb withdrawal was observed in both strains (Fig. 2C). Extracellular recording from the palmar nerve after light stimulation of the palmar skin revealed increased firing with increased length of light pulses (1, 10, or 50 ms), including C-fiber mass activity and maybe also A-fiber high-amplitude bursts (Fig. 2D). The low-threshold mechanoreceptors (LTMRs) terminating as lanceolate endings in hair follicles and innervating Merkel cells and Meissner corpuscles elicit sensations of hair deflection, touch, pressure, flutter, or vibration but not pain behavior (*9*). However, in chronic pain, light touch–activated neurons can contribute to mechanical allodynia (*10*–*12*). In contrast with Sox10-ChR2 positive control mice that displayed a robust light intensity–dependent response, optogenetic stimulation of LTMR terminal Schwann cells in Sox2-ChR2 mice failed to evoke a withdrawal response (Fig. 2C) and therefore do not contribute to the withdrawal response.

To ascertain that the reflexive defensive responses are caused by pain, we assayed coping behavior that may serve to soothe suffering (*13*). Optogenetic stimulation led to robust licking, shaking, and paw-guarding behavior (Fig. 3A).

To resolve the sensory modalities nociceptive Schwann cells modulate, optogenetic activation that is subthreshold to elicit behavior was combined with cold, heat, and mechanical stimuli. We reasoned that coincident subthreshold light could sensitize to the physiological stimuli that it modulates. Coping-behavior subthreshold stimulation significantly increased sharp 2-g von Frey coping behavior, whereas paw-withdrawal subthreshold stimuli did not affect touch sensitivity, measured by the cotton swab withdrawal assay (*14*) (Fig. 3, B and C), although they elevated the response to cold stimuli in both Plp-ChR2 and Sox10-ChR2 mice (Fig. 3, D and E, and fig. S5, B and C). In Sox10-ArchT mice generated to silence nociceptive Schwann cells, no difference in cold response was seen (Fig. 3F and fig. S5D). Withdrawal subthreshold optogenetic stimulation in Plp-ChR2 and Sox10-ChR2 potentiated heat-evoked

responses (Fig. 3, G and H, and fig. S5, A and E), but silencing did not result in any difference of the thermal threshold (Fig. 3I and fig. S5F). Plp-ChR2 mice displayed dose-dependent reduction of the mechanical withdrawal threshold by increasing the length of subthreshold light trains (Fig. 3J), confirmed in Sox10-ChR2 mice after coincident activation of Schwann cells (Fig. 3K and fig. S5G). Unlike for cold and heat, silencing resulted in a significantly increased mechanical threshold, which was reversed after 24 hours (Fig. 3L and fig. S5H).

Electrical properties of nociceptive Schwann cells were examined in dissociated Sox10-TOM–expressing nociceptive Schwann cells by whole-cell current-clamp electrophysiological recordings. Stepwise current injections revealed two-phase linear I-V relationships around the resting membrane potential (Fig. 4, A and B), with a clear knee precisely around their resting membrane potential (average of −32.56 ± 1.36 mV) (Fig. 4C). The decreased resistance upon depolarization (Fig. 4, D and E) indicates an intrinsic (nonmechanical) opening of channels, pulling the membrane potential toward resting value. The passive membrane properties indicated a slow time constant, within the range of neurons (Fig. 4F).

We measured electrical responses to mechanical stimuli to determine whether nociceptive Schwann cells are mechanically active. Whole-cell voltage response to mechanical force in steps of 40 nm with five or 10 steps at ~60 Hz, a pause, and thereafter five or 10 steps out was measured. Mechanical stimulation produced a transient depolarization (n = 9) (Fig. 4, G and H). Four cells did not return all the way to baseline, possibly because of the mechanical force affecting the integrity of the seal. In the remaining cells, the decay was essentially complete during continued force application, suggesting that the mechanoreceptive response adapts to sustained force over time. Both response and adaptation were very rapid, resulting in similar responses in the subsequent stimuli. The cells tracked the maximum frequency of stimuli that we could generate (60 Hz). Releasing the force also depolarized the cells (Fig. 4G). Thus, nociceptive Schwann cells responded to both positive and negative changes in force but much less to sustained force. Peak mean amplitude was 25.5 ± 2.1 mV (Fig. 4I), and 50% depolarization duration (half-width) was 6.7 ± 1.5 ms (Fig. 4J), with time at the beginning of the rising phase to the peak (rise time) of 1.4 ± 0.2 ms (Fig. 4K). This time course of the mechanoreceptor potential may reflect that of the underlying mechanoreceptor current. This suggests very fast gating mechanisms, similar to what has been described in sensory neurons (*15*, *16*).

We provide evidence for a specialized glial cell type that builds a sensory organ in the skin, initiating the sensation of pain. The nociceptive Schwann cells display a mesh-like network of cytoplasmic sheaths around nerves in the subepidermal border with radial processes entering into the epidermis abutting to unmyelinated nociceptive nerves. The nociceptive Schwann cells are the cellular equivalents of the ignored Remak Schwann

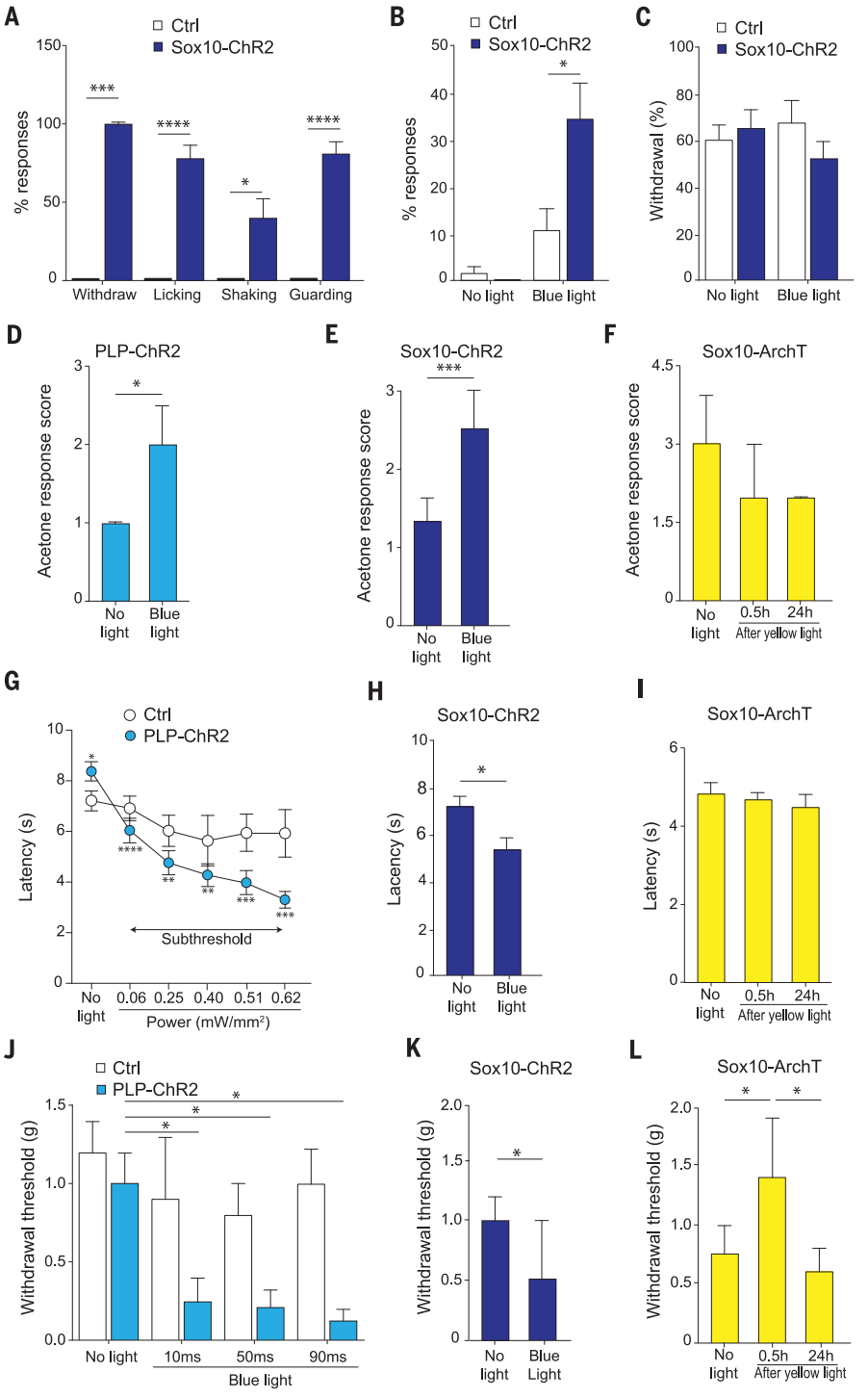

Fig. 3. Nociceptive Schwann cells determine the sensitivity threshold for mechanosensation. (**A**) Suprathreshold photoactivation of nociceptive Schwann cells evokes coping behavior associated with pain. (**B** to **L**) Blue bars, subthreshold optogenetic activation of nociceptive Schwann cells combined with natural stimuli and yellow bars before and after optogenetic inhibition. (B) Coping response to nociceptive mechanical stimuli (2-g von Frey). (C) Withdrawal to cotton swab. (D to F) Response to cold. (G to I) Withdrawal latency to heat. (J) Mechanical threshold without light or with increased length of subthreshold blue-light trains. (K) Mechanical threshold. (L) Mechanical threshold before or after optogenetic inhibition. Ctrl, control. Statistics text and *P* values can be found in the supplementary materials, material and methods.

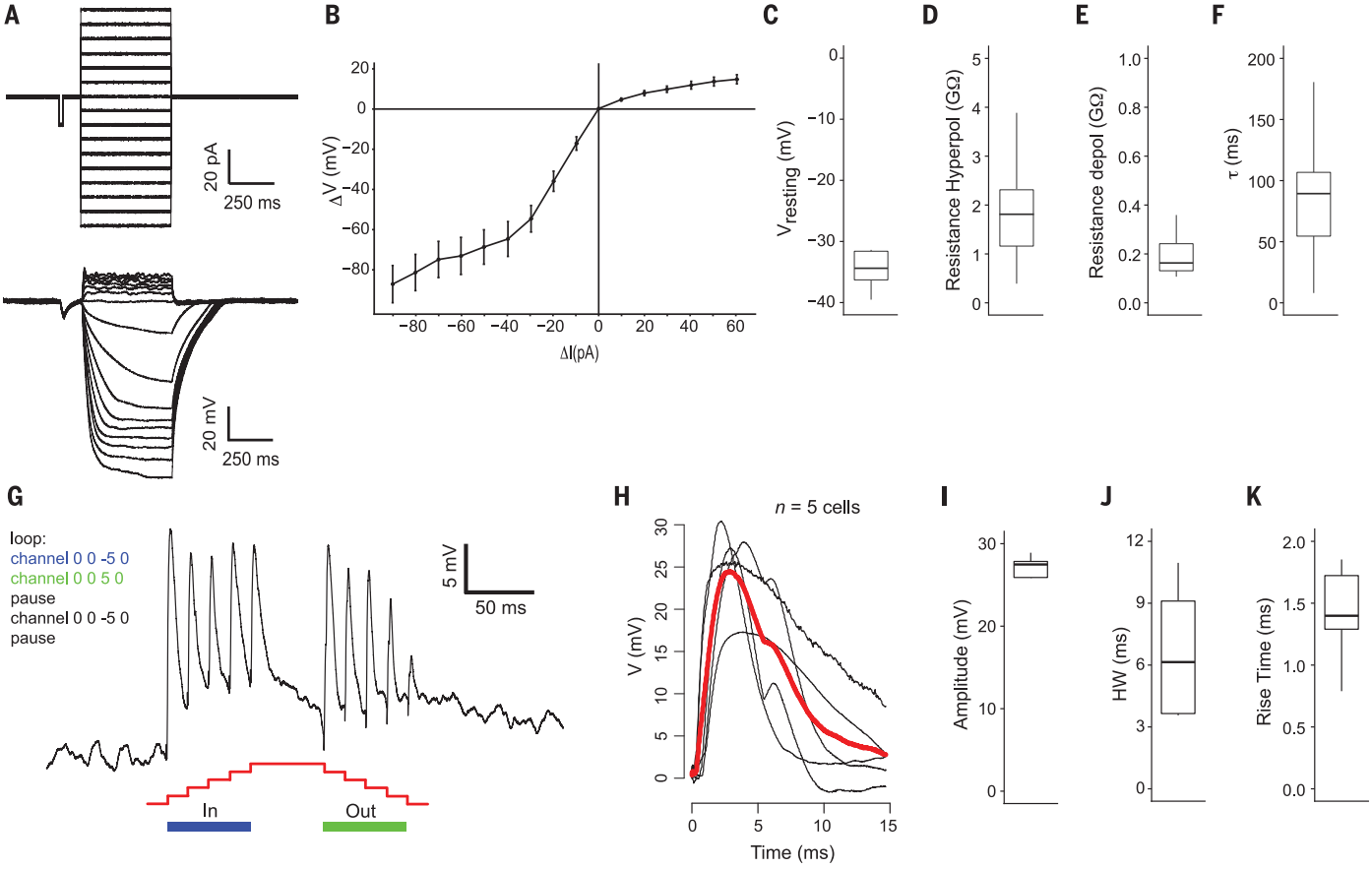

Fig. 4. Nociceptive Schwann cells are mechanosensory cells. (**A**) Voltage signal detected during whole-cell current-clamp recordings evoked current steps. (**B**) Two-phase linear I-V relationships during hyperpolarization and depolarization. (**C**) Resting membrane potential of nociceptive Schwann cells. (**D**) Resistance of cells calculated during hyperpolarizing current injections. (**E**) Resistance of cells calculated during depolarizing current injections. (**F**) Time constant (τ). (**G**) Mechanical stimulation of nociceptive Schwann cells during whole-cell current-clamp recordings; example of inward steps and subsequent outward steps applied as indicated. (**H**) Mechanically evoked depolarization (red, average). (**I**) Amplitudes of depolarization. (**J**) Half-width of depolarization. (**K**) 10 to 90% rise time of the depolarization. depol, depolarization; HW, half-width; Hyperpol, hyperpolarization.

cells described in the subepidermal border of the skin some 45 years ago. At that time, nerve fibers were thought to lose their glia attachment and enter epidermis as free nerve endings (*17*). The nociceptive Schwann cells are highly mechanosensitive with rapid adaptation and respond to both positive and negative changes in force, similar to "on" and "off" mechanoreceptor responses observed in *Caenorhabditis elegans* (*18*). They transduce nociceptive stimuli into electrical signals that translate into pain-like behavior. The nociceptive nerve endings in skin also gate responses to various noxious stimuli (*1*–*6*). Hence, nociceptive nerves and nociceptive Schwann cells form a nociceptive glio-neural complex with two sensor-receptor cell types, the glia and the nerve, both likely influencing the sensation of pain. Most or all types of nociceptors appear to contribute to the nociceptive glio-neural complex, and consistently, both mechanical and thermal nociception is potentiated in gain-of-function experiments. However, loss-of-function experiments indicate either that activation of thermosensitive ion channels in primary afferents (*19*–*22*) is sufficient by itself or, alternatively, that nociceptive Schwann cells contribute to a submodality not captured in our behavioral tests. By contrast, nociceptive Schwann cells are physiologically contributing to sensation of mechanical stimuli, as the threshold was affected in both gain- and loss-of-function experiments. This could suggest a broader response profile of discrete nociceptive neuron types than that predicted from their molecular profiles (*23*–*26*). Functional implications of our findings are vast if nerve and glial cell receptor types mediate different aspects of thermal and mechanical nociceptive transduction, as has been proposed for Merkel cells participating in non-noxious touch sensation (*27*–*29*).

REFERENCES AND NOTES

1. V. E. Abraira, D. D. Ginty, *Neuron* **79**, 618–639 (2013).
2. M. Costigan, J. Scholz, C. J. Woolf, *Annu. Rev. Neurosci.* **32**, 1–32 (2009).
3. F. Lallemend, P. Ernfors, *Trends Neurosci.* **35**, 373–381 (2012).
4. Y. Liu, Q. Ma, *Curr. Opin. Neurobiol.* **21**, 52–60 (2011).
5. C. Peirs *et al.*, *Neuron* **87**, 797–812 (2015).
6. S. A. Prescott, Q. Ma, Y. De Koninck, *Nat. Neurosci.* **17**, 183–191 (2014).
7. B. L. Harty, K. R. Monk, *Curr. Opin. Neurobiol.* **47**, 131–137 (2017).
8. K. R. Jessen, R. Mirsky, *J. Physiol.* **594**, 3521–3531 (2016).
9. C. J. Woolf, T. P. Doubell, *Curr. Opin. Neurobiol.* **4**, 525–534 (1994).
10. R. Dhandapani *et al.*, *Nat. Commun.* **9**, 1640 (2018).
11. M. Koltzenburg, L. E. Lundberg, H. E. Torebjörk, *Pain* **51**, 207–219 (1992).
12. C. Peng *et al.*, *Science* **356**, 1168–1171 (2017).
13. T. Huang *et al.*, *Nature* **565**, 86–90 (2019).
14. S. S. Ranade *et al.*, *Nature* **516**, 121–125 (2014).
15. K. Poole, R. Herget, L. Lapatsina, H. D. Ngo, G. R. Lewin, *Nat. Commun.* **5**, 3520 (2014).
16. Y. Song *et al.*, *J. Physiol. Biochem.* **74**, 207–221 (2018).
17. N. Cauna, *J. Anat.* **115**, 277–288 (1973).
18. R. O'Hagan, M. Chalfie, M. B. Goodman, *Nat. Neurosci.* **8**, 43–50 (2005).
19. M. J. Caterina *et al.*, *Nature* **389**, 816–824 (1997).
20. D. D. McKemy, W. M. Neuhausser, D. Julius, *Nature* **416**, 52–58 (2002).
21. A. M. Peier *et al.*, *Cell* **108**, 705–715 (2002).
22. I. Vandewauw *et al.*, *Nature* **555**, 662–666 (2018).
23. C. Li, S. Wang, Y. Chen, X. Zhang, *Neurosci. Bull.* **34**, 200–207 (2018).
24. C. L. Li *et al.*, *Cell Res.* **26**, 83–102 (2016).
25. D. Usoskin *et al.*, *Nat. Neurosci.* **18**, 145–153 (2015).
26. A. Zeisel *et al.*, *Cell* **174**, 999–1014.e22 (2018).
27. R. Ikeda *et al.*, *Cell* **157**, 664–675 (2014).

28. S. Maksimovic *et al*., *Nature* **509**, 617–621 (2014).
29. S. H. Woo *et al*., *Nature* **509**, 622–626 (2014).

ACKNOWLEDGMENTS

We thank M. Karlén for schematic illustrations. **Funding**: P.E. received the ERC (PainCells 740491), the Swedish MRC, KAW Scholar and project grant, and Welcome Trust (200183). M.-D.Z. received a brain foundation post-doc fellowship. **Author contributions**: Conceptualization: P.E. and I.A.; mouse models/behavior/experimental design: H.A. and L.C.-E.; electrophysiology: J.M.L. and J.H.-L.; nerve recording: J.S. and A.E.M.; Immuno: H.A., L.C.-E., and M.-D.Z.; animal platforms: D.U.; writing (H.A., L.C.-E., and P.E.) and revision (L.C.-E. and P.E.) of the manuscript with input from all authors: L.C.-E. and P.E.; and supervision and funding: P.E. **Competing interests**: No competing interests. **Data and materials availability:** All data are available in the manuscript or the supplementary material. The Sox10-CreERT2 mice were obtained under an MTA from MRC.

SUPPLEMENTARY MATERIALS

science.sciencemag.org/content/365/6454/695/suppl/DC1
Materials and Methods
Supplementary Text
Figs. S1 to S5

10 April 2019; accepted 2 July 2019
10.1126/science.aax6452

Science

Specialized cutaneous Schwann cells initiate pain sensation

Hind Abdo, Laura Calvo-Enrique, Jose Martinez Lopez, Jianren Song, Ming-Dong Zhang, Dmitry Usoskin, Abdeljabbar El Manira, Igor Adameyko, Jens Hjerling-Leffler and Patrik Ernfors

Science **365** (6454), 695-699.
DOI: 10.1126/science.aax6452

A newly discovered cell type for pain perception

Pain has been thought to be initiated by activation of free nerve endings without end organs in the skin. In contrast to this paradigm, Abdo *et al.* discovered a previously unknown meshlike organ covering the skin that senses dangerous environmental stimuli (see the Perspective by Doan and Monk). This organ is built from specialized glial cells located in the epidermal-dermal border and is sufficient and required for initiation of mechanical pain transduction.

Science, this issue p. 695; see also p. 641

Supplementary Materials for

Specialized cutaneous Schwann cells initiate pain sensation

Hind Abdo*, Laura Calvo-Enrique*, Jose Martinez Lopez, Jianren Song, Ming-Dong Zhang, Dmitry Usoskin, Abdeljabbar El Manira, Igor Adameyko, Jens Hjerling-Leffler, Patrik Ernfors†

*These authors contributed equally to this work.
†Corresponding author. Email: patrik.ernfors@ki.se

Published 16 August 2019, *Science* **365**, 695 (2019)
DOI: 10.1126/science.aax6452

This PDF file includes:

Materials and Methods

Mouse strains

All animal work was permitted by the Ethical Committee on Animal Experiments (Stockholm North committee) and conducted according to The Swedish Animal Agency's Provisions and Guidelines for Animals Experimentation recommendations. Mice of both sexes and from mixed background were used in this study. Animals were kept in cages in groups, with food and water *ad libitum,* under 12h light-dark cycle conditions. $Sox10^{CreERT2}$ mouse strain has been previously described (*Laranjeira et al., (2011) J Clin Invest Sept;121(9);3412-24, doi:10.1172/JCI58200*). $Plp^{CreERT2}$ (stock number 005975), $Sox2^{CreERT2}$ (stock number 017593), $Rosa26R^{YFP}$ (stock number 006148), $Rosa26R^{tdTomato}$ (Ai14, stock number 007914), $Rosa26R^{ChR2\text{-}EYFP}$ (Ai32, stock number 012569) and $Rosa26R^{ArchT\text{-}EGFP}$ (Ai40D, stock number 021188) were ordered from The Jackson Laboratory. $Plp^{CreERT2}$, $Sox10^{CreERT2}$ and $Sox2^{CreERT2}$ mice were coupled to $R26R^{YFP}$ and $R26R^{TOM}$ mice for tracing experiments and to $R26R^{ChR2}$ and $R26R^{ArchT}$ for behavioral and functional experiments. The resulting strains from the crosses were the following: $Plp^{CreERT2/+}$;$R26R^{EYFP/+}$ (abbreviated Plp-YFP), $Sox10^{CreERT2/+}$;$R26R^{TOM/+}$ (abbreviated Sox10-TOM), $Plp^{CreERT2/+}$;$R26R^{ChR2/+}$ (abbreviated Plp-ChR2), $Sox10^{CreERT2/+}$;$R26R^{ChR2/+}$ (abbreviated Sox10-ChR2), $Sox2^{CreERT2/+}$;$R26R^{ChR2/+}$ (abbreviated Sox2-ChR2), $Sox10^{CreERT2/+}$;$R26R^{ArchT/+}$ (abbreviated Sox10-ArchT). The animals used have a mixed genetic background (C57BL6, 6J, 6N).

Tamoxifen (Sigma, T5648) was dissolved in corn oil (Sigma, 8267) at a concentration of 20 mg/ml and delivered by intra peritoneal (i.p.) injection to adult for two consecutive days and only one injection to pups (100mg/kg pups and 200mg/kg adults). Controls and test mice received tamoxifen injections. Behavioral tests were

performed 7 days after the last tamoxifen injection.

Tissue preparation

Adult mice were sacrificed with isoflurane overdose and transcardially perfused with 20 ml PBS and 20 ml 4% paraformaldehyde (PFA, Roth, #P087.3). Paws, shaved back skin, sciatic or cutaneous nerve and lumbar dorsal root ganglia (DRG) were then collected and post-fixed in PFA (1h for DRG and nerves, 2h for paws and skin) at 4°C, washed 3 times with PBS and cryoprotected by incubating at 4°C in 30% sucrose in PBS with 0.02% sodium azide for 24h. Plantar/palmar skin of each paw was then dissected out, and tissue was embedded in OCT compound (Tissue-Tek) and frozen at -20°C. Tissue samples were sectioned at 14 or 20 µm thickness and conserved at –20°C until further use.

For electron microscopy, plantar skin of hindpaws were dissected out and fixed by immersion in 2% glutaraldehyde and 1% paraformaldehyde for transmission electron microscopy or 3% paraformaldehyde for immune-electron microscopy.

Immunohistochemistry

Thawed sections were air dried for at least one hour at room temperature (RT). Antigen retrieval was performed for SOX10 stainings and Merkel cell identification in the skin. For that, sections were immersed in 1x Target Retrieval Solution (Dako, #S1699) in water for 20 min, pre-heated at 80°C. Sections were then washed two times in PBS and incubated in blocking solution (5% normal donkey serum (NDS, Jackson Immuno Research, #017-000-121), 2% Bovine Serum Albumin (BSA, Sigma, #A7906), 0.3% Triton X-100 in PBS) for 1h before applying primary antibodies overnight at 4°C. The following primary antibodies (diluted in the blocking

solution) were used: rabbit anti–PGP9.5 (1:1000, AbD Serotec, #7863-0504), goat anti-GFP-FITC (1:1000, Abcam, #ab6662), chicken anti-GFP (1:500, Aves Labs Inc., #GFP-1020), goat anti-SOX10 (1:200, Santa Cruz, #sc-17342), rabbit anti-S100β (1:500, Dako, #Z0311), rabbit anti-DsRed (1:300, Clontech, #632496), chicken anti-NF200 (1:10000, Abcam, #ab4680), rat anti-CK8 (1:50, DSHB, TROMA1), rabbit anti-MBP (1:500, Dako, #A062301), mouse anti-Aqp1 (1:100, Santa Cruz, #sc-25287 (B11)), rabbit anti-TRPV1 (1:2000, Santa Cruz, #sc-28759), rabbit anti-P2X3 (1:5000, Abcam, #ab10269), guinea pig anti-TLX3 (kind gift from T. Müller, 1:10 000) and rabbit anti-CGRP (1:50 000, kind gift from Tomas Hökfelt). CGRP, P2X3 and TRPV1 were visualized using the TSA Plus Kit (PerkinElmer) according to manufacturer´s instructions.

For detection of the primary antibodies, secondary antibodies raised in donkey and conjugated with Alexa-488, -555, -594 and -647 fluorophores were used (1:1000, Molecular Probes, ThermoFisher Scientific) for 1h at RT.

Dapi staining (1mg/ml, ThermoFisher Scientific, #D1306) was performed as the same time as secondary antibodies. Sections were then washed 3 times with PBS and mounted using fluorescent mounting medium for imaging (Dako, #S3023).

Images were acquired using Zeiss LSM700 confocal microscope equipped with 20x, 40x and 63x objectives. Images were acquired in the .lsm format and processed with ImageJ. Representative images are maximum intensity projections of Z-stacks taken at 1μm intervals.

Electron microscopy

For transmission electron microscopy (TEM), skin samples were fixed by immersion in 2% glutaraldehyde and 1% paraformaldehyde in 0.1 M PB for 24 h at 4°C, washed

with 0.1M PB and post-fixed in 2% osmiumtetroxide (OsO4) in 0.1 M PB for 2h at 4°C. Samples were then dehydrated by incubation in ethanol, followed by acetone before embedding in epoxy resin LX-112 (Ladd, Burlington, VT). Semi-thin sections were first made and stained with toluidine blue for light microscopy analysis. Ultrathin sections were made with Leica Ultracut UCT (Leica, Vienna, Austria), contrasted with uranyl and examined in a Tecnai 10 Transmission electron microscope at 80 kV (FEI company). Digital images were made using a MegaViewIII digital camera (soft imaging system, GmbH, Münster, Germany). For immuno electron microscopy (iEM), skin samples were fixed in 3% paraformaldehyde and 2% glutaraldehyde in 0.1 M PB for 24h at 4°C. TEM and iEM images were in main but not supplementary figures pseudo-colored using Adobe Photoshop for visualization of neuronal and glial structures. EM microscopy has been done in the Center for high resolution electron microscopy core facility (Department of Bioscience and Nutrition, Karolinska Institutet).

Terminal Schwann cell dissociation and culture

Terminal Schwann cells were obtained from glabrous skin of Sox10-TOM P11-P14 pups (at least 96h after tamoxifen administration). Briefly, pups were sacrificed with isoflurane overdose; paws were quickly collected in ice cold HBSS medium (ThermoFisher Scientific, #14170112) containing 100 U/ml penicillin, 100 ug/ml streptomycin (supplied as a mix, ThermoFisher Scientific, #15140122). Plantar skin was then dissected out from each paw, and after removal of nerves and other tissues, skin was incubated in fresh HBSS containing 4 mg/ml of collagenase/dispase (Sigma-Aldrich, cat.11097113001) for 30 min at 37°C. Epidermis was then removed and the dermis, after careful removal of footpads, was cut in small pieces and incubated with

4 mg/ml of collagenase/elastase (Worthington. Cat. LK002066) in HBSS for 30 min at 37°C. DNAse I was added (Worthington. Cat. LK003170) to a final concentration of 1 mg/ml before mechanical dissociation with fire polished Pasteur pipettes coated previously with 1% BSA in PBS. The cell suspension was slowly filtered through 40 μm-pore size cell strainer and centrifuged at 300 g for 6 min. The pellet was re-suspended in Schwann cell medium (DMEM with D-valine (Miclev, #AL251) supplemented with 2 mM glutamine (ThermoFisher Scientific, #23030081), 10% Fetal Bovine Serum (Sigma, #2442), 1% N2 (Life Technologies, #17502001), 100 U/ml penicillin, 100 μg /ml streptomycin and 20 μg/ml bovine pituitary extract (Sigma, #P1476). Cells were plated on coverslips coated with poly-L-lysine (Sigma, P4707) for 2 h at 37°C and then with laminin (Sigma, #L2020) for 30 min at 37°C. Culturing took place in humidified 5%CO_2/95% air atmosphere.

Behavior studies

All behavioral tests were performed on adult mice (2-4 months) from both sexes and their corresponding littermates were used as controls (not expressing the drivers but only the reporters).

Excitatory optogenetic coping behavior and threshold measurement: After habituation on a metal mesh floor, Plp-ChR2, Sox10-ChR2 and Sox2-ChR2 mice and their correspondent control littermates (without expression of Cre^{ERT2}) were stimulated with blue light pulses (470nm, 10 Hz, 50 ms, 10 pulses) applied through a flexible fiber optic bundle to restrict the illumination to the intended skin area with 90° angle on the plantar surface of both hindpaws (consequently) with increasing light power. Mice were tested five times on each paw with at least 3 min between left and right paws and at least 10 minutes between two trials on the same paw.

Light threshold was determined as the lowest light power provoking a nocifensive response in one of the paws. Subthreshold light stimulations (0.06 mW/mm^2) were then applied simultaneously with other stimuli. For thermal pain tests, light threshold was determined using the thermal pain testing platform by applying the light under the glass surface at a 45° angle. In all experiments, light was applied simultaneously with below tests.

Acute light-evoked pain coping behavior: After habituation on a mesh floor, Sox10-ChR2 mice and their correspondent littermates (without Cre^{ERT2} expression) were stimulated with blue light pulses (470 nm, 10 Hz, 50 ms, 10 pulses, 1.98 mW/mm^2) on a plantar surface of the hindpaws. Paw withdrawal, paw licking, paw shaking and paw guarding were measured.

Cotton swab assay: Response to a gentle stroke was assessed by stroking dynamically a cotton swab on the plantar surface of the hindpaw. Mice were acclimated on a mesh-floor and a cotton swab with the cotton "puffed out" manually such that the cotton head became 3 times bigger than its original size. We performed a quick stroke along the plantar paw 4 times, alternating between paws, and recorded the number of paw withdrawals and reported as percentage for each mouse. Subthreshold light stimulation is 0.06 mW/mm^2, 10 Hz, 50 ms, 10 pulses.

Response to 2g von Frey filament:. After habituation on a mesh floor, Sox10-ChR2 mice and their correspondent littermates (without Cre^{ERT2} expression) were stimulated with a 2g von Frey filament and coping behavior such as licking, shaking or guarding was quantified. Then 2g von Frey was applied simultaneously with coping behavior subthreshold light stimulation (0.20 mW/mm^2, 10 Hz, 50 ms, 10 pulses). Responses was reported as percentage of animals with a coping behavior response.

Mechanical threshold: After a resting period on a mesh floor, the plantar surface of the hindpaws were stimulated with a series of calibrated monofilaments (von Frey hairs; Stoelting, IL, USA) with increasing force until the desired responses were elicited. Each filament was applied five times. The withdrawal threshold was defined as the force at which the animal withdrew the paw at least three out of the five trials. Thereafter withdrawal threshold was measured with simultaneous application of von Frey filaments and subthreshold light stimuli on the same paw area. Subthreshold light stimulation is 0.06 mW/mm^2, 10 Hz, 50 ms, 10 pulses if not otherwise stated in the figure or figure legend.

Hargreaves' test: A radiant heat source (IITC, Woodland Hills, CA, USA) was aimed at the plantar surface of the hindpaw through a glass surface. Readout was the withdrawal latency of the stimulated paw. Thereafter withdrawal threshold was measured with simultaneous application of radiant heat source and subthreshold light stimuli. Subthreshold light stimulation is 0.06 mW/mm^2, 10 Hz, 50 ms, 10 pulses.

Acetone evaporation assay**:** The acetone evaporation assay was performed using the scoring method. Briefly, mice were first acclimated on a mesh surface. Then the plantar skin of the hind paw was gently contacted with an acetone drop formed at the tip of a 1 ml syringe. Response to acetone cooling effect was scored from 0 to 5 according to the following scale: 0 = no response, 1 = brief lift, sniff, flick, or startle; 2 = jumping, paw shaking; 3 = multiple lifts, paw lick; 4 = prolonged paw lifting, licking, shaking, or jumping; 5 = paw guarding. Mice were tested five times on each paw with a waiting time of 2 minutes between. Acetone response score was then measured on a different day simultaneously with subthreshold blue light. Subthreshold light stimulation is 0.06 mW/mm^2, 10 Hz, 50 ms, 10 pulses.

Inhibitory optogenetics. To test the effect of silencing terminal Schwann cells, mechanical and thermal sensitivities were assessed before and after yellow light (575 nm, 30 min) stimulation. Sox10-ArchT or control littermates (without Cre^{ERT2} expression) were anesthetized with 1% isofluorane meanwhile the light was applied to the plantar surface of the hindpaw with a 5s on, 1 s off pulsing frequency. The light beam (0.5 mW/mm^2) covered the entire plantar surface. Mechanical and thermal sensitivities were measured before and after 30 min and 24 h post-stimulation. Contralateral paws without any optical stimulation were considered as internal controls for the anesthesia. ArchT is a light-driven outward proton pump which could acidify the capillary cleft between Schwann and nerve cell and we cannot exclude that this could exert unspecific effects on nerve terminals. Acidification would be predicted to have excitatory effects on nerves, as protons are known to activate nociceptors and this occurs at least in part through TRPV1 and ASICs. However, our results show an inhibitory effect on the nerve which is the opposite of what one would expect if the behavioral effects were caused by protons in the capillary cleft. Furthermore, any effect on the nerve, whether excitatory or inhibitory, would be the same regardless if combined with on Frey, cold or heat. Our results show that inactivation of nociceptive glia through ArchT does not affect cold and heat thresholds, while von Frey thresholds are increased. Thus, we conclude that the recorded behavioral effect of glia inactivation on mechanical threshold is very unlikely to be caused by protons pumped out of the ArchT.

Extracellular recording from the paw nerve

Recording from the nerve was performed on paws from Sox10-ChR2 mice. Briefly, forepaws and hindpaws were collected in extracellular solution at 4°C, and under the

microscope, the plantar or palmar skin was opened in hindpaws and forepaws respectively, nerves innervating the corresponding limb were identified (tibial nerve in the hindpaw and palmar nerve in the forepaw). The paw was then perfused with air bubbled extracellular solution for 30-60 min at room temperature before recording. After that the nerve of interest was sucked in the electrode and the electrical activity was recorded following application of blue light (470 nm; 0.4 mW/mm^2; 5Hz) on the skin through a 10x objective. Ten pulses were applied with increasing durations (1, 10 and 50 ms). The analysis of the electrophysiological data was performed using Spike2 (Cambridge Electronic Design) or Clampfit (Molecular Devices) software. Responses were successfully obtained in two out of six animals.

Whole-cell electrophysiology

Whole-cell patch-clamp current clamp recordings on cultured terminal Schwann cells from Sox10-Tom mice were conducted at 2-5 DIV. Electrophysiological recordings of $TOMATO^+$ cells were performed using Multiclamp 700B amplifier (Molecular Devices) and analyzed off-line in Clampfit and R.

Bath solution contained (in mM): 125 NaCl, 2.5 KCl, 25 $NaHCO_3$, 1.25 NaH_2PO_4, 1 $MgCl_2$, $2CaCl_2$, 20 glucose and 20 HEPES. Patch pipettes had a tip resistance of 4-6 MΩ. The internal solution of the pipette contained the following (in mM): 105 K-gluconate, 30 KCl, 10 Na-Phosphocreatine, 10 HEPES, 4 Mg-ATP, 0.3 Na-GTP and pH adjusted to 7.27 with KOH. The temperature of the bath was 24-28 °C.

Depolarizing and hyperpolarizing current steps were used to extract the electrical properties of terminal Schwann cells. Resistance of the cell was calculated by performing a linear fit to I-V curve in the phases of hyperpolarization and depolarization. Membrane time constant was calculated by performing an exponential

fit to the decay phase of voltage response to a negative current step.

Mechanical stimulation was performed using Kleindiek nanotechnik MM3A Micromanipulator with a glass probe affixed to the piezoelectrically-driven actuator. Movements of the mechanical probe were executed using the next commands sent to the controller in loop mode:

channel 0 0 -S 0

channel 0 0 S 0

pause T

channel 0 0 -S 0

pause T

where S was 5 or 10 steps in the in/out axis of the device and T was a value between 0.25 and 1 s. Mechanical probes were custom-made with patch pipettes heated for 10 s with a microforge (Narishige MF-90). Measurements of halfwidth and amplitude in responding cells were carried out in a one representative mechanical spike of every cell showing at least one spike before breaking the seal (n=5 cells). 3 of these cells showed multiple spikes concomitant with mechanical stimuli.

Quantification and Statistics

Data were analyzed using GraphPad Prism 5 and expressed as mean ± standard error of the mean (SEM) or median ± median absolute deviation (MAD) (for acetone evaporation test and Von Frey assay). Statistical significance was calculated using 2-sided paired Student's *t*-test or Wilcoxon matched-pairs signed rank test (for parametric and non parametric data) and Mann-Whitney *U*-test when two different genotypes were compared. Degree of significance was represented as follow: * p-value ≤ 0.05; ** p-value ≤ 0.01; *** p≤ 0.001; **** p≤ 0.0001. No statistical methods

were used to predetermine sample size, but our sample sizes are similar to those generally employed in the field.

To assess the specificity of recombination in DRG, at least 400 recombined cells were counted in randomly selected lumbar DRG sections from 2-3 mice. In order to estimate the efficiency of recombination within terminal Schwann cells, $Tomato^{+}Sox10^{+}$ cells and total $Sox10^{+}$ cells were counted from five sections of glabrous skin per animal ($n = 3$).

P values:

Fig. 3A. Percentage paw withdraw control vs Sox10-ChR2, $n = 8$ per group, *** $P = 0.0002$, Mann-Whitney U test. Percentage paw licking control vs Sox10-ChR2, $n = 8$ per group, **** $P < 0.0001$, two tailed unpaired t test with Welch´s correction. Percentage paw shaking control vs Sox10-ChR2, $n = 8$ per group, * $P = 0.0138$, two tailed unpaired t test with Welch´s correction. Percentage paw guarding control vs Sox10-ChR2, $n = 8$ per group, **** $P < 0.0001$, two tailed unpaired t test with Welch´s correction. Data are presented as mean ± SEM.

Fig. 3B. Sox10-ChR2 without photostimulation vs Sox10-ChR2 with subthreshold photostimulation for coping behavior (0.20 mW/mm^2, 10 Hz, 50 ms, 10 pulses), $n = 8$. * $P = 0{,}0156$, two-tailed Wilcoxon matched-pairs signed rank test. Control mice without photostimulation vs control with subthreshold photostimulation for coping behavior, $n = 7$, no significant, $\underline{P} = 0.25$, two-tailed Wilcoxon matched-pairs signed rank test. Control mice with subthreshold photostimulation vs Sox10-ChR2 with subthreshold photostimulation, * $P = 0.0457$, Mann-Whitney U test. Data are presented as mean ± SEM.

Fig. 3C. Sox10-ChR2 without photostimulation vs Sox10-ChR2 with subthreshold photostimulation (0.06 mW/mm^2, 10 Hz, 50 ms, 10 pulses), $n = 9$, no significant, $P =$

0,1269, two-tailed paired student *t* test. Data are presented as mean ± SEM.

Fig. 3D. Plp-ChR2 without photostimulation vs Plp-ChR2 with subthreshold photostimulation (0.06 mW/mm^2, 10 Hz, 50 ms, 10 pulses), n = 11, * P = 0.0195, two-tailed Wilcoxon matched-pairs signed rank test. Data are presented as median ± MAD.

Fig. 3E. Sox10-ChR2 without photostimulation vs Sox10-ChR2 with subthreshold photostimulation (0.06 mW/mm^2, 10 Hz, 50 ms, 10 pulses), n = 12, *** P = 0.001, two-tailed Wilcoxon matched-pairs signed rank test. Data are presented as median ± MAD.

Fig. 3F. Sox10-ArchT without photostimulation vs Sox10- ArchT after 30 min with photostimulation (0.5 mW/mm^2, 5s on 1s off pulsing frequency, for 30 minutes), n = 7, no significant, P = 0.6250, two-tailed Wilcoxon matched-pairs signed rank test. Data are presented as median ± MAD.

Fig. 3G. Plp-ChR2 (n = 6) vs control littermates (n = 5) without photostimulation * P = 0.048, two-tailed unpaired Student's *t*-test with Welch's correction. Without photostimulation vs subthreshold photostimulation for Plp-ChR2 mice (n = 6): 0.06 mW/mm^2: * P = 0.011, 0.25 mW/mm^2: ** P = 0.0014, 0.40 mW/mm^2: ** P = 0.012; 0.51 mW/mm^2: *** P = 0.0002; 0.62 mW/mm^2: *** P < 0.0001, two-tailed paired Student's *t*-test. Data are presented as mean ± SEM.

Fig. 3H. Sox10-ChR2 without photostimulation vs Sox10-ChR2 with subthreshold photostimulation (0.06 mW/mm^2, 10 Hz, 50 ms, 10 pulses), n = 7, * P = 0.0332, two-tailed paired Student's *t*-test. Data are presented as mean ± SEM.

Fig. 3I. Sox10-ArchT without photostimulation vs Sox10- ArchT after 30 min with photostimulation (0.5 mW/mm^2, 5s on 1s off pulsing frequency, for 30 minutes), n =

10, non-significative, P = 0.6038, two-tailed paired Student's t-test. Data are presented as mean ± SEM.

Fig. 3J. Plp-ChR2 (n = 6) vs control littermates (n = 5) without photostimulation, non-significant, P = 0.2706, Mann-Whitney U test. Plp-ChR2 without photostimulation vs Plp-ChR2 subthreshold photostimulation (0.06 mW/mm^2, 10 Hz, 10 pulses), * P = 0.0313, two tailed Wilcoxon matched-pairs signed rank test. Data are presented as median ± MAD.

Fig. 3K. Sox10-ChR2 without photostimulation vs Sox10-ChR2 with subthreshold photostimulation (0.06 mW/mm^2, 10 Hz, 50 ms, 10 pulses), n = 7, * P = 0.0156, two tailed Wilcoxon matched-pairs signed rank test. Data are presented as median ± MAD.

Fig. 3L. Sox10-ArchT without photostimulation vs Sox10-ArchT after photostimulation (0.5 mW/mm^2, 5s on 1s off pulsing frequency, for 30 minutes), n = 10, * P = 0.0195 (no light vs 0.5h after light); * P = 0.0156 (0.5h vs 24h after light), two tailed Wilcoxon matched-pairs signed rank test. Data are presented as median ± MAD.

Fig. S5B. Plp-ChR2 without photostimulation vs Plp-ChR2 with subthreshold photostimulation (0.06 mW/mm^2, 10 Hz, 50 ms, 10 pulses), n = 11, * P = 0.0195, two-tailed Wilcoxon matched-pairs signed rank test. Control without photostimulation vs control with subthreshold photostimulation, n = 8, non-significant P = 0.75, two-tailed Wilcoxon matched-pairs signed rank test. Data are presented as median ± MAD.

Fig. S5C. Sox10-ChR2 without photostimulation vs Sox10-ChR2 with subthreshold photostimulation (0.06 mW/mm^2, 10 Hz, 50 ms, 10 pulses), n = 12, *** P = 0.001. Control without photostimulation vs control with subthreshold photostimulation, n =

10, non-significant $P = 0.6563$, two-tailed Wilcoxon matched-pairs signed rank test. Data are presented as median ± MAD.

Fig. S5D. Behavioral response to cold stimuli using acetone evaporation test score without (baseline) and with optogenetic inhibition applied (0.5 mW/mm^2, 5s on 1s off pulsing frequency, for 30 minutes), and measured 0.5h or 24h after in Sox10-ArchT ($n = 7$) and control littermates ($n = 6$) mice. No statistical significance between control (before light and any of states after light application), Wilcoxon matched-pairs signed rank test. Data are presented as median ± MAD.

Fig. S5E. Withdrawal latency to radiant heat (Hargreaves' assay) without or with subthreshold optogenetic stimulation in Sox10-ChR2 ($n = 7$) and control littermates (white bars, $n = 9$). Sox10-ChR2 without photostimulation vs Sox10-ChR2 with subthreshold photostimulation (0.06 mW/mm^2, 10 Hz, 50 ms, 10 pulses), $n = 7$, * $P = 0.0332$, two-tailed paired Student's *t*-test. Data are presented as mean ± SEM

Fig. S5F. Withdrawal latency to radiant heat (Hargreaves' assay) without (baseline) and with optogenetic inhibition applied (0.5 mW/mm^2, 5s on 1s off pulsing frequency, for 30 minutes), and measured after 0.5h or 24h in Sox10-ArchT ($n = 10$) and control littermates ($n = 8$) mice. Sox10-ArchT without photostimulation vs Sox10- ArchT after 30 min with photostimulation, $n = 10$, non-significative, $P = 0.6038$, two-tailed paired Student's *t*-test. Data are presented as mean ± SEM.

Fig. S5G. Mechanical threshold measured with von Frey filaments in Sox10-ChR2 ($n = 13$) and control littermate ($n = 13$) mice without light or with subthreshold blue light. Sox10-ChR2 without photostimulation vs Sox10-ChR2 with subthreshold photostimulation (0.06 mW/mm^2, 10 Hz, 50 ms, 10 pulses), * $P = 0.0156$, two tailed Wilcoxon matched-pairs signed rank test. Data are presented as median ± MAD.

Fig. S5H. Mechanical threshold measured with von Frey filaments in Sox10-ArchT (n = 10) and control littermate (n = 8) mice before (baseline) and 0.5h and 24h after yellow light application.. Sox10-ArchT without photostimulation vs Sox10-ArchT after photostimulation (0.5 mW/mm^2, 5s on 1s off pulsing frequency, for 30 minutes), n = 10, * P = 0.0195 (no light vs 0.5h after light); * P = 0.0156 (0.5h vs 24h after light), two tailed Wilcoxon matched-pairs signed rank test. Data are presented as median ± MAD.

Extended figure legends for main figures.

Fig. 1. Cutaneous Schwann cells form a glio-neural end-organ in the skin.

(A and B) Cutaneous Schwann cells in the sub-epidermal border with radial processes into epidermis ensheath unmyelinated nerve endings. Immunhistochemistry for GFP, TOMATO, PGP9.5, SOX10 and S100β. Genetically labeled Schwann cells in Plp-YFP (A) and Sox10-TOM (B) mice associate with unmyelinated nerves ($PGP9.5^{+}$) and express glial markers SOX10 and S100β. Insets show higher magnification. Scale bar in A-B: 10 μm. (**C** and **D**) Transmission electron microscopy of the glio-neural complex obtained from glabrous skin of Sox10-TOM mice. Images were pseudo-colored (axons, green pseudo-color and nociceptive Schwann cell and its processes, light red pseudo-color). (C1) Subepidermal border and (C2) epidermis are higher magnification of boxed area in (C). Arrowheads points to basal lamina on the abaxonal surface, characteristic of Schwann cells and arrows point to axons. (C3 and C4) Subepidermal Schwann cell processes enfold few (C4) or several axons (C3) really close to epidermis (red arrow is 1 μm in C4). (D) Immuno-electron microscopy with anti-dsRed antibody (red dots) shows specific expression of TOMATO in Schwann cell process and not by the axons. Scale bars, C and C1: 2 μm, C2: 500nm, C3 and C4: 2 μm, D: 500 nm. (**E**) Immunohistochemistry for Aquaporin1 (Aqp1) in glabrous skin of Sox10-TOM mice. Scale bar: 20 μm. (**F**) Immunohistochemistry for CGRP and P2X3 in glabrous skin of Sox10-TOM mice. Scale bar: 20 μm and 5 μm for the insets. (**G**) Schematic illustration of the glio-neural complex in the sub-epidermal border and epidermis (nociceptive Schwann cell, red and nerves, blue). e, epidermis; d, dermis; Sch, cutaneous Schwann cell; f, fibrillary collagen; n, nucleus; ax, axon; SCp, Schwann cell process. Hatched line indicates dermal-epidermal border.

Fig. 2. Nociceptive Schwann cells can initiate pain-like behavior and are sufficient to elicit action potential propagation.

(**A**) Immunohistochemistry for TOMATO, PGP9.5, NF200, MBP and CK8 reveals recombination in LTMR end-organ glia and in Remak glia of nerves in Sox10-TOM and Sox2-TOM mice, and in the latter also in Merkel cells. Immunostainings on sections of Sox10- TOM and Sox2-TOM mice. Scale bar: 10 μm. (**B**) Sox10-TOM but rarely Sox2-TOM mice recombine in nociceptive Schwann cells ($SOX10^+$). White arrows non-recombined, yellow arrow occasional recombined $SOX10^+$ Schwann cell in Sox2-TOM mice. Scale bar: 10μm. Quantification on right (n = 3, mean ± SEM). (**C**) Optogenetic stimulation of nociceptive Schwann cells results in nocifensive behavior. Sox10-ChR2 and Plp-ChR2 mice but not Sox2-ChR2 mice respond to blue light application on the plantar side of hindpaws (n = 6-8 mice per data point). (**D**) Activation of nociceptive Schwann cells results in nerve electrical activity. Extracellular recording from the median palmar nerve after optogenetic stimulation on the palmar skin of the forepaw of Sox10-ChR2 mice. Ten pulses (visualized as blue marks on the graph) of blue light (470 nm; 0.4 mW/mm^2) were applied on the whole surface of the paw through 10x objective. On state of pulses for each stimulation lasted 1 ms, 10 ms or 50 ms (left to right recordings).

Fig. 3. Nociceptive Schwann cells determine the sensitivity threshold for mechanosensation.

(**A**) Suprathreshold photo-activation of nociceptive Schwann cells evokes coping behavior associated to pain. Percent behavioral responses (paw withdrawal, paw licking, paw shaking and paw guarding) in Sox10-ChR2 (n = 8) and control littermates (n = 8) mice evoked by optogenetic stimulation (1.98 mW/mm^2, 50 ms, 10

Hz, 10 pulses) of the plantar surface of the hindpaws. (**B**) Percentage coping response to 2 g von Frey filament on the hindpaw in Sox10-ChR2 (*n* = 8) and control littermates (*n* = 7) without and with subthreshold optogenetic stimulation (0.20 mW/mm^2, 50 ms, 10 Hz, 10 pulses) applied simultaneously. (**C**) Percent withdrawal to cotton swab stroke on the hindpaw in Sox10-ChR2 (*n* = 9) and control littermate (*n* = 8) mice without and with subthreshold optogenetic stimulation (0.06 mW/mm^2, 50 ms, 10 Hz, 10 pulses) applied simultaneously. (**D)** Response to acetone evaporation test on Plp-ChR2 (*n* = 11) mice without and with subthreshold optogenetic stimulation (0.06 mW/mm^2, 50 ms, 10 Hz, 10 pulses) applied simultaneously. **(E**) Response to acetone evaporation test without and with subthreshold optogenetic stimulation (0.06 mW/mm^2, 50 ms, 10 Hz, 10 pulses) applied simultaneously in Sox10-ChR2 (*n* = 12) mice. (**F**) Behavioral response to cold using acetone evaporation test score before and after optogenetic inhibition (0.5 mW/mm^2, 5s on 1s off pulsing frequency, for 30 minutes), in Sox10-ArchT mice (*n* = 7). (**G**) Heat withdrawal latency in Plp-ChR2 (*n* = 6) or control littermates (*n* = 5) without light or in combination with increasing blue light power. (**H**) Withdrawal latency to radiant heat (Hargreaves' assay) in Sox10-ChR2 mice (*n* = 7) without or with subthreshold optogenetic stimulation (0.06 mW/mm^2, 50 ms, 10 Hz, 10 pulses). (**I**) Withdrawal latency to radiant heat (Hargreaves' assay) in Sox10-ArchT mice (*n* = 10) before or after optogenetic inhibition. (**J**) Mechanical threshold measured with von Frey filaments in Plp-ChR2 (*n* = 6) or control littermate (*n* = 5) mice without light or with increased length of subthreshold blue light trains (0.06 mW/mm^2, 10 Hz, 10 pulses). (**K**) Mechanical threshold measured with von Frey filaments in Sox10-ChR2 mice (*n* = 7) without or with subthreshold blue light (0.06 mW/mm^2, 50 ms, 10 Hz, 10 pulses). (**L**) Mechanical threshold measured with von Frey filaments in Sox10-ArchT

mice (n = 10) before or after optogenetic inhibition (0.5 mW/mm^2, 5s on 1s off pulsing frequency, for 30 minutes).

Figure 4. Nociceptive Schwann cells are mechanosensory cells.

(**A**) Voltage signal detected during whole-cell current clamp recordings evoked by 500 ms current steps. Nociceptive Schwann cells do not show electrical firing patterns upon depolarizing current steps. (**B**) Two-phase linear I/V relationships during hyperpolarization and depolarization of nociceptive Schwann cells (n = 17 cells). The slopes of linear fits give the resistance of cells according to Ohm's Law V = RI. (**C**) Resting membrane potential (-32.56 ± 1.36 mV, mean ± SEM) of nociceptive Schwann cells (NSC). Box-plot showing median and quartiles. (**D**) Resistance of cells calculated during hyperpolarizing current injections (between -20 and 0 pA) (1.80 ± 0.24, mean ± SEM, n = 17). Box-plot showing median and quartiles. (**E**) Resistance of cells calculated during depolarizing current injections (between 0 and 60 pA) (0.24 ± 0.04, mean ± SEM, n = 17). The resistance during depolarization is lower than during hyperpolarization. Box-plot showing median and quartiles. (**F**) Time-constant τ of nociceptive Schwann cells (82.53 ± 11.36, mean ± SEM, n = 17). Box-plot showing median and quartiles. (**G**) Mechanical stimulation of nociceptive Schwann cells identified by Tomato fluorescence using a custom-made round tip glass-pipette during whole-cell current clamp recordings. Example of 5 inward steps (40 nm each) and 5 subsequent outward steps applied as indicated. All spikes were concomitant with the mechanical probe movements. (**H**) Representative mechanically evoked depolarization from 5 cells. Thick red line shows the average of transients. (**I**) Amplitudes of the depolarization in the recorded cells. Box-plot showing median and quartiles. **(J)** Half-width of depolarization. Box-plot showing median and quartiles.

(K) 10% to 90 % rise time of the depolarization. Box-plot showing median and quartiles.

Supplementary figures and legends

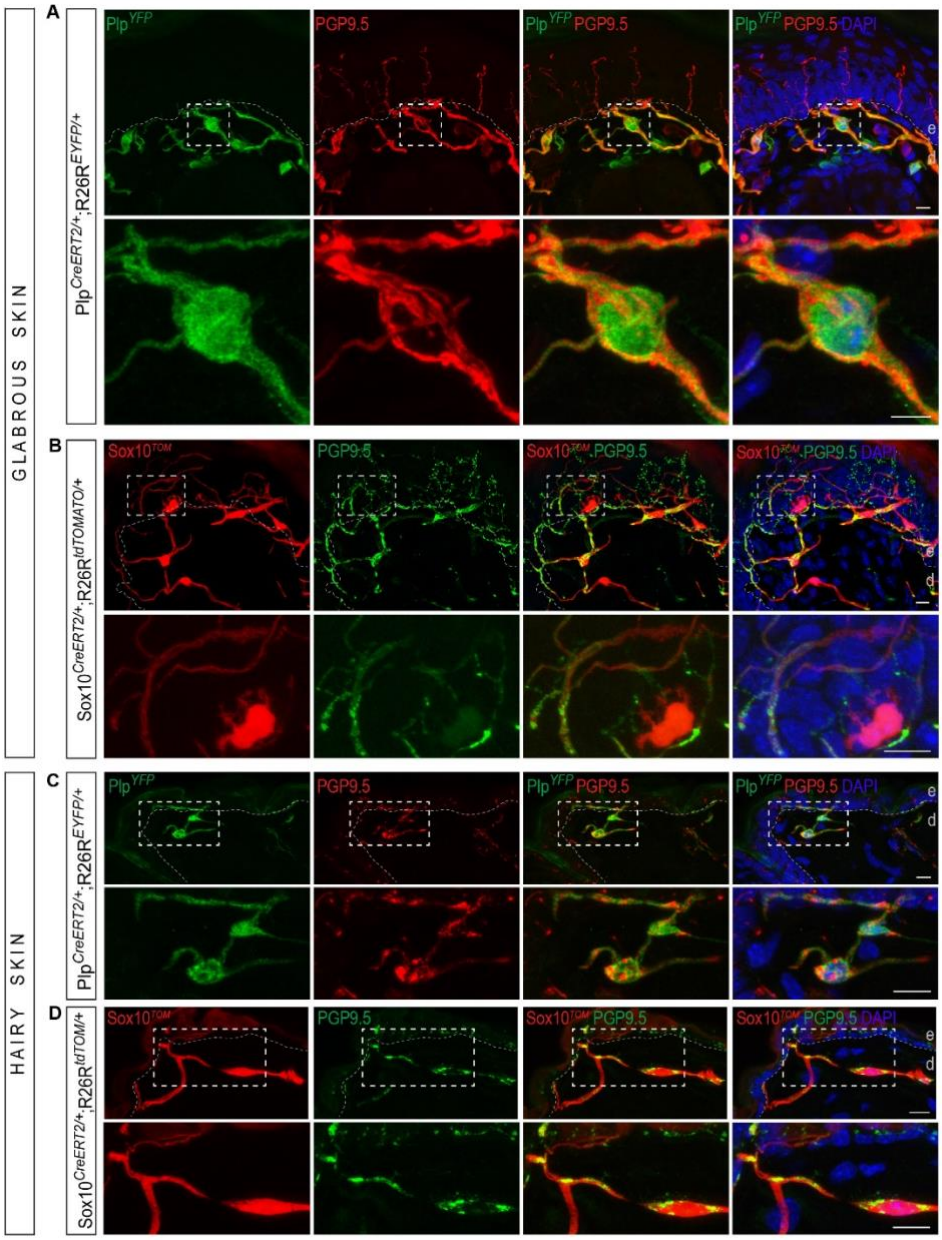

Fig. S1. Nociceptive Schwann cells are located in the sub-epidermal border with radial epidermal processes in both glabrous and hairy skin.

(**A**) Immunohistochemistry for YFP (recapitulating *Plp* expression) and for PGP9.5 detecting nerves on glabrous skin of Plp-YFP mice shows that nociceptive Schwann cells are intimately associated with unmyelinated nerve endings in the sub-epidermal border. Enlargements in panel A are boxed in the lower magnification images. (**B**) Immunohistochemistry for TOMATO (recapitulating *Sox10* expression) and for PGP9.5 on glabrous skin of Sox10-TOM shows also how nociceptive

Schwann cells are penetrating the epidermis abutted to nerve endings. Enlargements in panel B are boxed in the lower magnification images. (**C**) Immunohistochemistry for YFP (recapitulating *Plp* expression) and for PGP9.5 on hairy skin of Plp-YFP. Enlargements in panel C is boxed in the lower magnification images. (**D**) Immunohistochemistry for TOMATO (recapitulating *Sox10* expression) and for PGP9.5 on hairy skin of Sox10-TOM. Enlargements in panel D are boxed in the lower magnification images. In all images, border between dermis and epidermis is outlined by hatched line. e: epidermis; d: dermis. Scale bar: 10 μm.

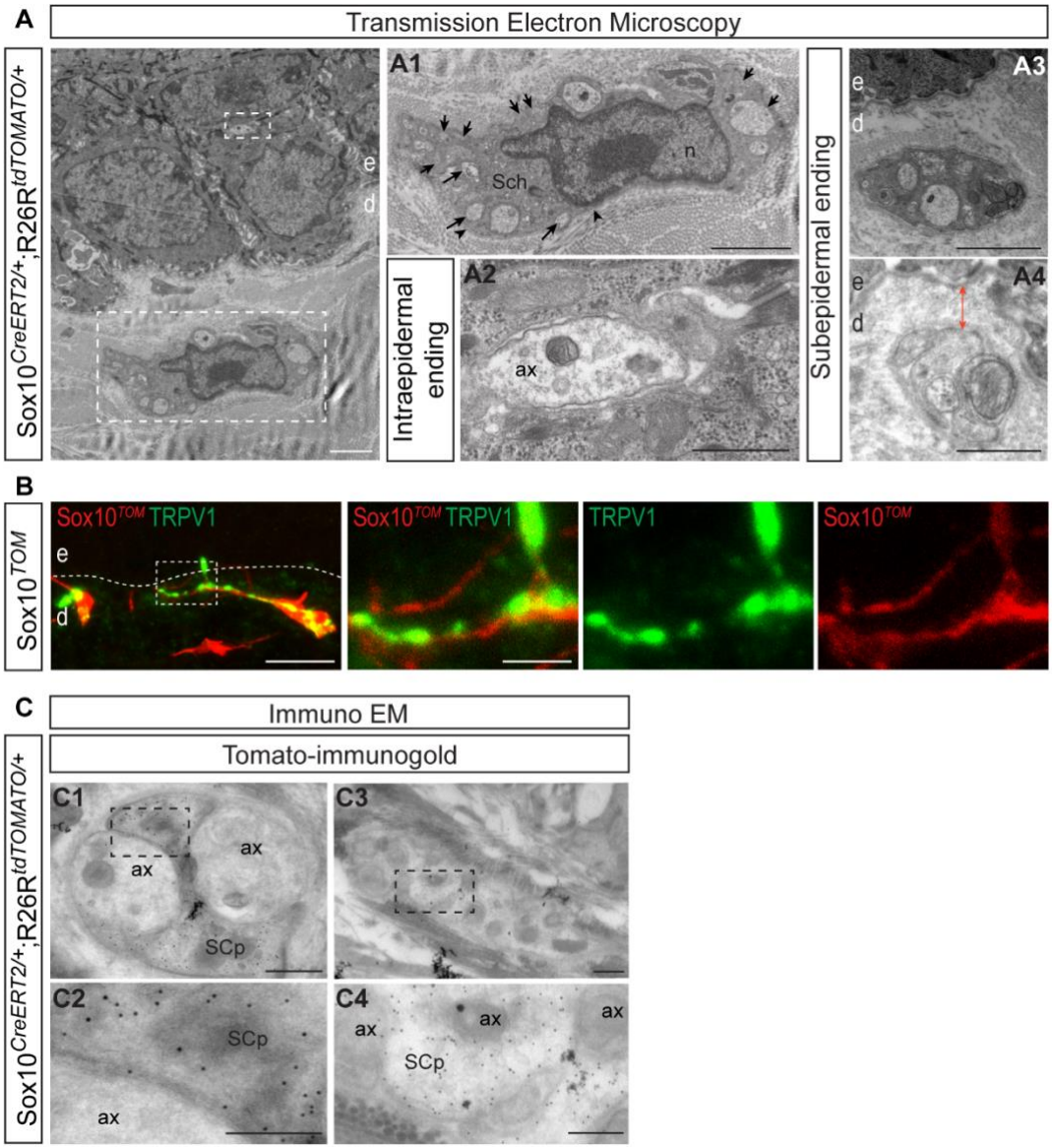

Fig. S2. Nociceptive Schwann cells ensheath nerve endings in the epidermal-dermal boundary and penetrate into the epidermis abutting unmyelinated neurites.

Non-pseudo-colored images of main Figure 1C and D. (**A**) Transmission electron microscopy images obtained from glabrous skin of Sox10-TOM mice. Micrographs showing the morphology of a nociceptive Schwann cell located in the vicinity (2-3 μm) of the epidermis and embracing several axons within its cytoplasm. (**A1**) Enlargement of A. Black arrows show axons inside the nociceptive Schwann cell. Arrowheads point basal lamina on the abaxonal surface, characteristic of Schwann cells. Arrows point to axons. (**A2**) Intra-epidermal nerve ending associated with a thin process of Schwann cell cytoplasm abutting the nerve. (**A3-A4**) Micrographs showing nociceptive Schwann cell processes ensheathing several axons (A3) or a single axon

(A4). Distance to epidermis is less than 1 μm (white arrow). (**B**) Immunohistochemistry for Tomato (recapitulating Sox10 expression) and for TRPV1 detecting peptidergic nerves on glabrous skin of Sox10-TOM mice. Scale bar: 20 μm, and 5 μm for the inset. (**C1-C4**) Immuno-electron microscopy with anti-dsRed antibody and revealed with immuno-gold coupled secondary antibody (dark dots). Tomato is specifically expressed in nociceptive Schwann cell processes (SCp) and not by the axons (ax). (**C2**) Enlargement of inset in C1. (**C4**) Enlargement of inset in C3. e, epidermis; d, dermis; Sch, nociceptive Schwann cell; n, nucleus; ax, axon; SCp, Schwann cell process. Scale bar in A, A1, A3 and A4: 2 μm, in A2, C1 and C3: 500nm in C2 and C4: 250nm.

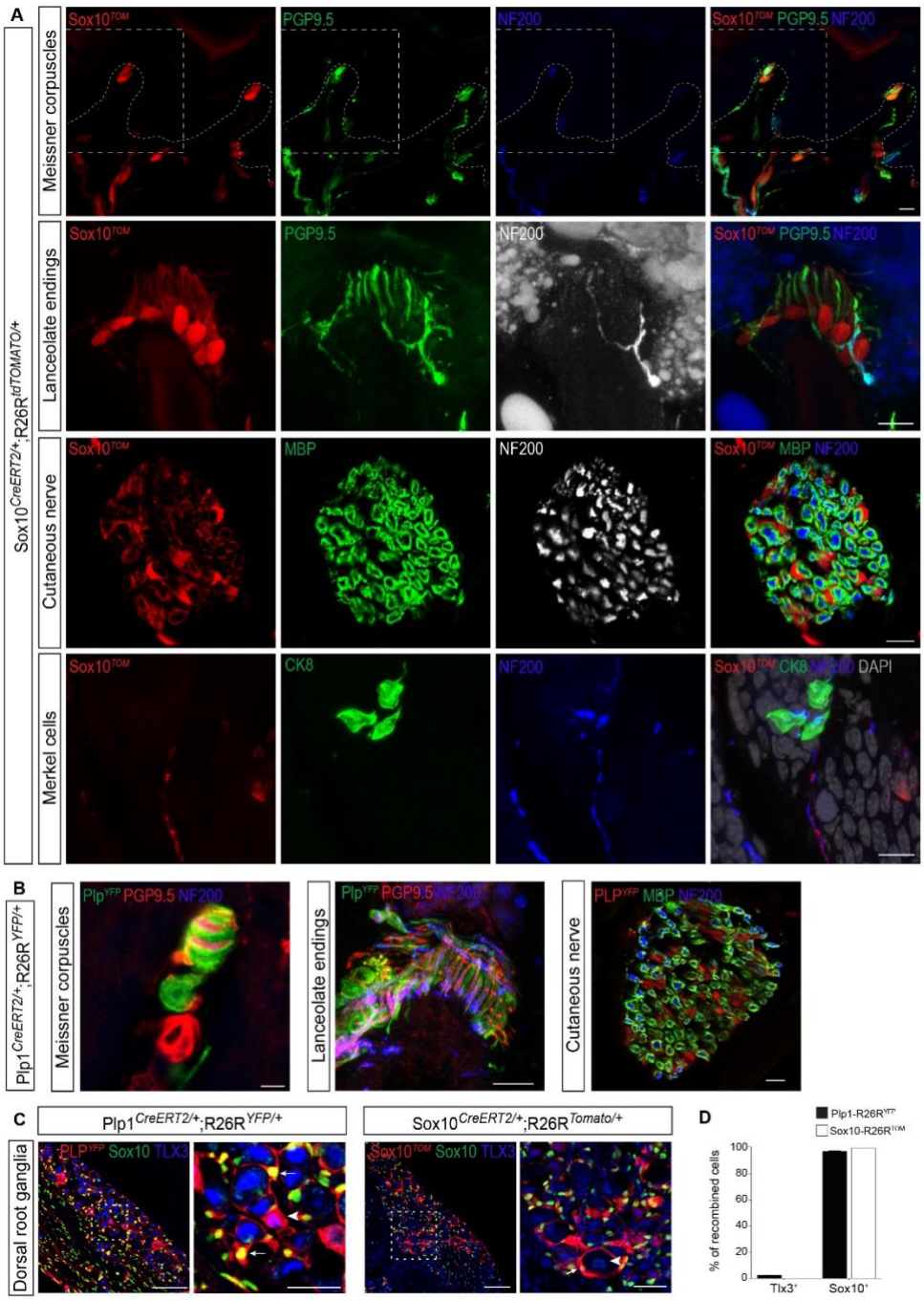

Fig. S3. Recombination in end-organs, cutaneous nerve and dorsal root ganglia in Plp-YFP and Sox10-TOM mice.

(**A**) Recombination in glial cells of Meissner corpuscles and lanceolate endings and in cutaneous nerve but not in Merkel cells in Sox10-TOM mice. Immunohistochemistry for TOMATO (recapitulating *Sox10* expression), for PGP9.5 and NF200 in Meissner corpuscles and lanceolate endings. Immunohistochemistry for TOMATO

(recapitulating *Sox10* expression), for MBP and for NF200 in cutaneous nerve. Immunohistochemistry for TOMATO (recapitulating *Sox10* expression), for CK8 in Merkel cells and NF200 for nerves. Higher magnification of panel A recapitulates image presented in Figure 2A for Meissner corpuscles. Dashed line indicates dermal-epidermal border. Scale bar: 10 μm. (**B**) Recombination in Meissner corpuscles and lanceolate endings and in cutaneous nerve in Plp-YFP mice. Immunohistochemistry for YFP (recapitulating *Plp* expression), for PGP9.5 and for NF200 in Meissner corpuscles and lanceolate endings. Immunohistochemistry for YFP (recapitulating *Plp* expression), for MBP and for NF200 in cutaneous nerve. Scale bar: 10 μm. (**C**) Recombination in dorsal root ganglia neurons in Plp-YFP and Sox10-TOM mice. Immunohistochemistry for YFP in Plp-YFP mice and for TOMATO in Sox10-TOM mice and for both strains immunohistochemistry for Sox10 (to detect satellite glia) and TLX3 (to detect all neurons). Arrows indicate satellite glial cells around neurons and arrowheads indicate neurons. Recombination is evident in satellite glia occasionally in neurons of Plp-YFP mice while no recombination at all was observed in neurons of Sox10-TOM mice. Scale bar: 100 μm (**D**) Quantification of recombination in dorsal root ganglia satellite glia ($SOX10^+$) and neurons ($TLX3^+$) of Plp-YFP (n = 3) and Sox10-TOM mice (n = 2). Data are presented as mean ± SEM (for Plp-YFP and just mean for Sox10-TOM).

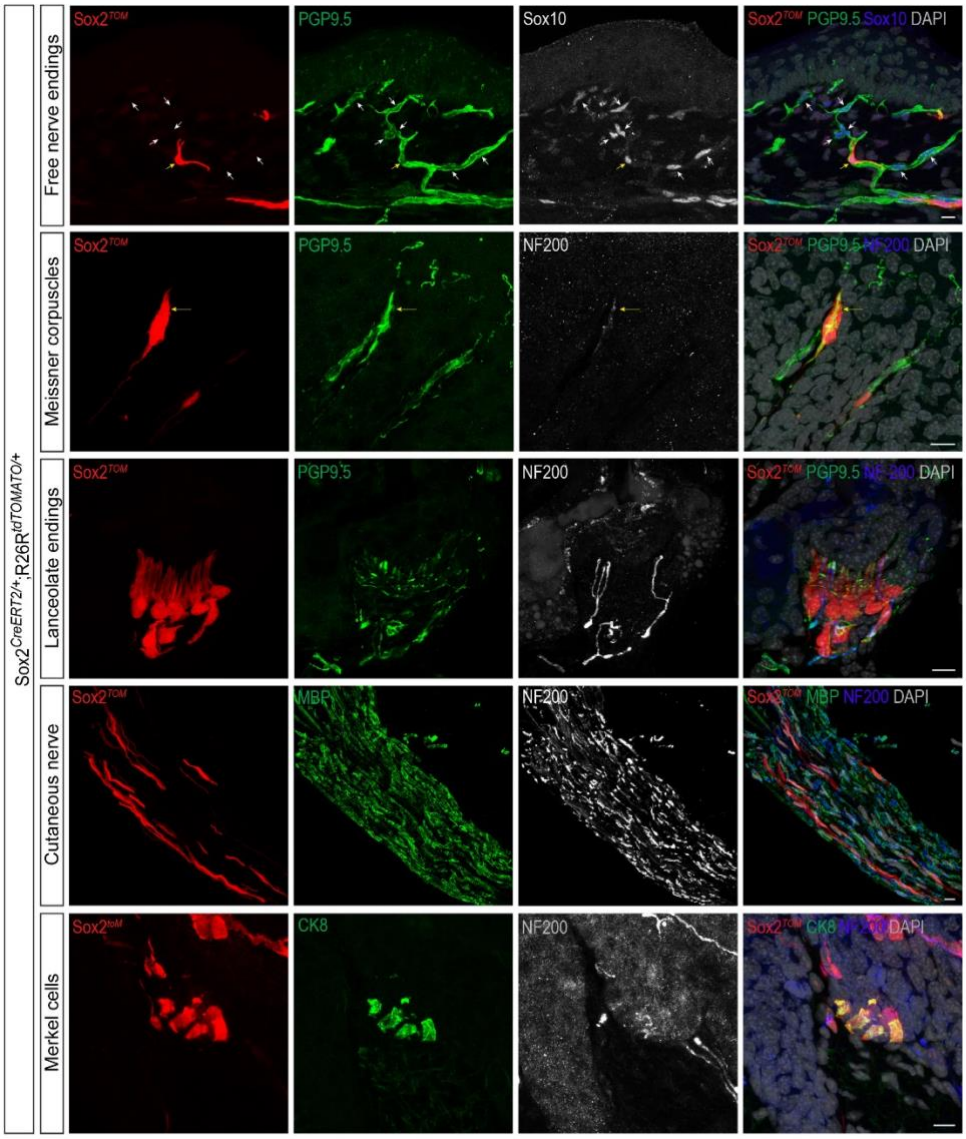

Fig. S4. Recombination in Meissner, lanceolate and Merkel end-organs but not in nociceptive Schwann cells of Sox2-TOM mice.

Separated channel images of Figure 2A and B. Immunohistochemistry for TOMATO (recapitulating *Sox2* expression), for PGP9.5 and for SOX10 in nociceptive Schwann cells that ensheath nerve endings (arrows). Immunohistochemistry for TOMATO, for PGP9.5 and for NF200 in Meissner corpuscles and lanceolate endings. Immunohistochemistry for TOMATO, for MBP and for NF200 in cutaneous nerve. Immunohistochemistry for TOMATO, for CK8 and for NF200 in Merkel cells. Note recombination in Meissner corpuscles, in lanceolate endings, in Merkel cells and in cutaneous nerve but rarely in nociceptive Schwann cells in Sox2-TOM mice. Scale bar: 10 μm.

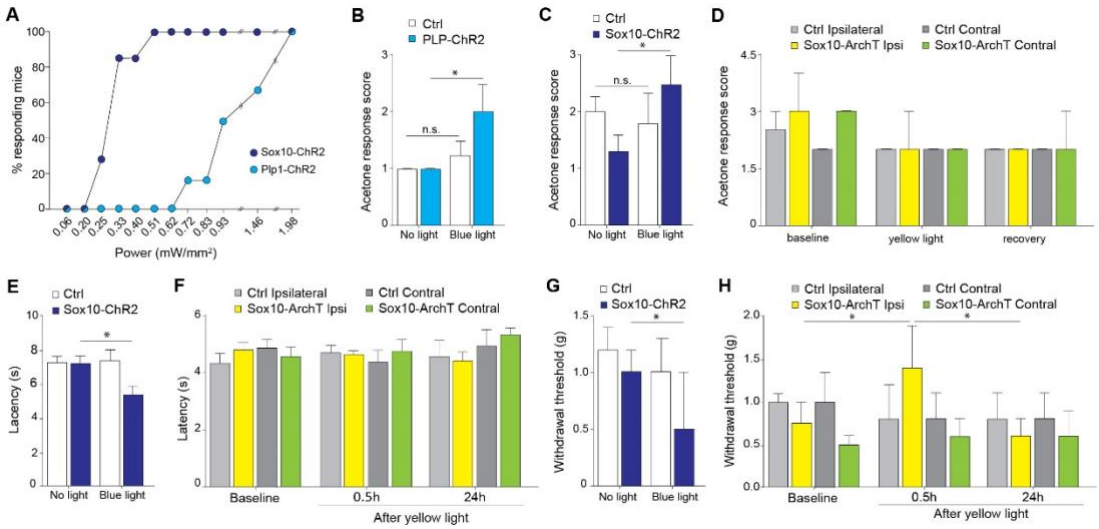

Fig. S5. Photostimulation or photoinhibition of nociceptive Schwann cells tunes pain behavior.

(A) Percentage of mice responding to optogenetic stimulation of the hindpaw through a glass floor (5mm thickness) with increasing light power in Plp-ChR2 (light blue) and Sox10-ChR2 (dark blue) strains. Each data point represents one measurement performed on six to eight mice.

(**B-C**) Behavioral response to cold stimuli using acetone evaporation test with and without subthreshold optogenetic stimulation applied simultaneously in Plp-ChR2 (B, light blue bars, n = 11) and control littermate mice (white bars, n = 8) * P = 0.0195, two-tailed, paired, Wilcoxon test and in Sox10-ChR2 (C, dark blue bars, n = 12) and control littermates (white bars, n = 10), *** P = 0.001, two-tailed, paired, Wilcoxon test.

(**D**) Behavioral response to cold stimuli using acetone evaporation test score without (baseline) and with optogenetic inhibition applied 0.5h (yellow) or 24h (recovery) before in Sox10-ArchT (n = 7) and control littermates (n = 6) mice. No statistical significance between control (before light and any of states after light application), Wilcoxon matched-pairs signed rank test.

(**E**) Withdrawal latency to radiant heat (Hargreaves' assay) without or with subthreshold optogenetic stimulation in Sox10-ChR2 (blue dark bars, n = 7) and control littermates (white bars, n = 9). * P = 0.0332, two-tailed, paired, Student's t test.

(**F**) Withdrawal latency to radiant heat (Hargreaves' assay) without (baseline) and with optogenetic inhibition applied 0.5h (yellow) or 24h (recovery) before in Sox10-ArchT (n = 10) and control littermates (n = 8) mice.

(**G**) Mechanical threshold measured with von Frey filaments in Sox10-ChR2 (n = 13) and control littermate (n = 13) mice without light or with subthreshold blue light. * P = 0.0156 two-tailed, paired, Wilcoxon test.

(**H**) Mechanical threshold measured with von Frey filaments in Sox10-ArchT (n = 10) and control littermate (n = 8) mice before (baseline) and 0.5h (yellow) and 24h (recovery) after yellow light application. * P = 0.0195 (baseline vs 0.5h after light) * P = 0.0156 (0.5h vs 24h after light), two-tailed, paired, Wilcoxon test.

References and Notes

1. V. E. Abraira, D. D. Ginty, The sensory neurons of touch. *Neuron* **79**, 618–639 (2013).

2. M. Costigan, J. Scholz, C. J. Woolf, Neuropathic pain: A maladaptive response of the nervous system to damage. *Annu. Rev. Neurosci.* **32**, 1–32 (2009).

3. F. Lallemend, P. Ernfors, Molecular interactions underlying the specification of sensory neurons. *Trends Neurosci.* **35**, 373–381 (2012).

4. Y. Liu, Q. Ma, Generation of somatic sensory neuron diversity and implications on sensory coding. *Curr. Opin. Neurobiol.* **21**, 52–60 (2011).

5. C. Peirs, S.-P. G. Williams, X. Zhao, C. E. Walsh, J. Y. Gedeon, N. E. Cagle, A. C. Goldring, H. Hioki, Z. Liu, P. S. Marell, R. P. Seal, Dorsal Horn Circuits for Persistent Mechanical Pain. *Neuron* **87**, 797–812 (2015).

6. S. A. Prescott, Q. Ma, Y. De Koninck, Normal and abnormal coding of somatosensory stimuli causing pain. *Nat. Neurosci.* **17**, 183–191 (2014).

7. B. L. Harty, K. R. Monk, Unwrapping the unappreciated: Recent progress in Remak Schwann cell biology. *Curr. Opin. Neurobiol.* **47**, 131–137 (2017).

8. K. R. Jessen, R. Mirsky, The repair Schwann cell and its function in regenerating nerves. *J. Physiol.* **594**, 3521–3531 (2016).

9. C. J. Woolf, T. P. Doubell, The pathophysiology of chronic pain—Increased sensitivity to low threshold A beta-fibre inputs. *Curr. Opin. Neurobiol.* **4**, 525–534 (1994).

10. R. Dhandapani, C. M. Arokiaraj, F. J. Taberner, P. Pacifico, S. Raja, L. Nocchi, C. Portulano, F. Franciosa, M. Maffei, A. F. Hussain, F. de Castro Reis, L. Reymond, E. Perlas, S. Garcovich, S. Barth, K. Johnsson, S. G. Lechner, P. A. Heppenstall, Control of mechanical pain hypersensitivity in mice through ligand-targeted photoablation of TrkB-positive sensory neurons. *Nat. Commun.* **9**, 1640 (2018).

11. M. Koltzenburg, L. E. Lundberg, H. E. Torebjörk, Dynamic and static components of mechanical hyperalgesia in human hairy skin. *Pain* **51**, 207–219 (1992).

12. C. Peng, L. Li, M.-D. Zhang, C. Bengtsson Gonzales, M. Parisien, I. Belfer, D. Usoskin, H. Abdo, A. Furlan, M. Häring, F. Lallemend, T. Harkany, L. Diatchenko, T. Hökfelt, J. Hjerling-Leffler, P. Ernfors, miR-183 cluster scales mechanical pain sensitivity by regulating basal and neuropathic pain genes. *Science* **356**, 1168–1171 (2017).

13. T. Huang, S.-H. Lin, N. M. Malewicz, Y. Zhang, Y. Zhang, M. Goulding, R. H. LaMotte, Q. Ma, Identifying the pathways required for coping behaviours associated with sustained pain. *Nature* **565**, 86–90 (2019).

14. S. S. Ranade, S.-H. Woo, A. E. Dubin, R. A. Moshourab, C. Wetzel, M. Petrus, J. Mathur, V. Bégay, B. Coste, J. Mainquist, A. J. Wilson, A. G. Francisco, K. Reddy, Z. Qiu, J. N. Wood, G. R. Lewin, A. Patapoutian, Piezo2 is the major transducer of mechanical forces for touch sensation in mice. *Nature* **516**, 121–125 (2014).

15. K. Poole, R. Herget, L. Lapatsina, H. D. Ngo, G. R. Lewin, Tuning Piezo ion channels to detect molecular-scale movements relevant for fine touch. *Nat. Commun.* **5**, 3520 (2014).

16. Y. Song, M. Zhang, X. Tao, Z. Xu, Y. Zheng, M. Zhu, L. Zhang, J. Qiao, L. Gao, Difference of acute dissociation and 1-day culture on the electrophysiological properties of rat dorsal root ganglion neurons. *J. Physiol. Biochem.* **74**, 207–221 (2018).

17. N. Cauna, The free penicillate nerve endings of the human hairy skin. *J. Anat.* **115**, 277–288 (1973).

18. R. O'Hagan, M. Chalfie, M. B. Goodman, The MEC-4 DEG/ENaC channel of Caenorhabditis elegans touch receptor neurons transduces mechanical signals. *Nat. Neurosci.* **8**, 43–50 (2005).

19. M. J. Caterina, M. A. Schumacher, M. Tominaga, T. A. Rosen, J. D. Levine, D. Julius, The capsaicin receptor: A heat-activated ion channel in the pain pathway. *Nature* **389**, 816–824 (1997).

20. D. D. McKemy, W. M. Neuhausser, D. Julius, Identification of a cold receptor reveals a general role for TRP channels in thermosensation. *Nature* **416**, 52–58 (2002).

21. A. M. Peier, A. Moqrich, A. C. Hergarden, A. J. Reeve, D. A. Andersson, G. M. Story, T. J. Earley, I. Dragoni, P. McIntyre, S. Bevan, A. Patapoutian, A TRP channel that senses cold stimuli and menthol. *Cell* **108**, 705–715 (2002).

22. I. Vandewauw, K. De Clercq, M. Mulier, K. Held, S. Pinto, N. Van Ranst, A. Segal, T. Voet, R. Vennekens, K. Zimmermann, J. Vriens, T. Voets, A TRP channel trio mediates acute noxious heat sensing. *Nature* **555**, 662–666 (2018).

23. C. Li, S. Wang, Y. Chen, X. Zhang, Somatosensory Neuron Typing with High-Coverage Single-Cell RNA Sequencing and Functional Analysis. *Neurosci. Bull.* **34**, 200–207 (2018).

24. C. L. Li, K.-C. Li, D. Wu, Y. Chen, H. Luo, J.-R. Zhao, S.-S. Wang, M.-M. Sun, Y.-J. Lu, Y.-Q. Zhong, X.-Y. Hu, R. Hou, B.-B. Zhou, L. Bao, H.-S. Xiao, X. Zhang, Somatosensory neuron types identified by high-coverage single-cell RNA-sequencing and functional heterogeneity. *Cell Res.* **26**, 83–102 (2016).

25. D. Usoskin, A. Furlan, S. Islam, H. Abdo, P. Lönnerberg, D. Lou, J. Hjerling-Leffler, J. Haeggström, O. Kharchenko, P. V. Kharchenko, S. Linnarsson, P. Ernfors, Unbiased classification of sensory neuron types by large-scale single-cell RNA sequencing. *Nat. Neurosci.* **18**, 145–153 (2015).

26. A. Zeisel, H. Hochgerner, P. Lönnerberg, A. Johnsson, F. Memic, J. van der Zwan, M. Häring, E. Braun, L. E. Borm, G. La Manno, S. Codeluppi, A. Furlan, K. Lee, N. Skene, K. D. Harris, J. Hjerling-Leffler, E. Arenas, P. Ernfors, U. Marklund, S. Linnarsson, Molecular Architecture of the Mouse Nervous System. *Cell* **174**, 999–1014.e22 (2018).

27. R. Ikeda, M. Cha, J. Ling, Z. Jia, D. Coyle, J. G. Gu, Merkel cells transduce and encode tactile stimuli to drive Aβ-afferent impulses. *Cell* **157**, 664–675 (2014).

28. S. Maksimovic, M. Nakatani, Y. Baba, A. M. Nelson, K. L. Marshall, S. A. Wellnitz, P. Firozi, S.-H. Woo, S. Ranade, A. Patapoutian, E. A. Lumpkin, Epidermal Merkel cells are mechanosensory cells that tune mammalian touch receptors. *Nature* **509**, 617–621 (2014).

29. S. H. Woo, S. Ranade, A. D. Weyer, A. E. Dubin, Y. Baba, Z. Qiu, M. Petrus, T. Miyamoto, K. Reddy, E. A. Lumpkin, C. L. Stucky, A. Patapoutian, Piezo2 is required for Merkel-cell mechanotransduction. *Nature* **509**, 622–626 (2014).